AVA analysis and geological dip estimation via two-way wave-equation based extended images

Rajiv Kumar, Tristan van Leeuwen and Felix J. Herrmann*
**University of British Columbia, Department of Earth, Ocean and Atmospheric Sciences*

SUMMARY

In this paper, we present an efficient way to compute extended images for *all* subsurface offsets without explicitly calculating the source and receiver wavefields for *all* the sources. Because the extended images contain *all* possible subsurface offsets, we compute the angle-domain image gathers by selecting the subsurface offset that is aligned with the local dip. We also propose a method to compute the local dip information directly from common-image-point gathers. To assess the quality of the angle-domain common-image-points gathers we compute the angle-dependent reflectivity coefficients and compare them with theoretical reflectivity coefficients yielded by the (linearized) Zoeppritz equations for a few synthetic models.

INTRODUCTION

Seismic imaging is very challenging in areas, where complexities of velocity model cause multipathing. Wave-equation based migration handles multipathing of the reflected energy naturally because the solution of the wave-equation is not computed as a finite set of high-frequency arrivals but the whole wavefield is propagated at each step of a wavefield-continuation process (Biondi (2003)). One such wave-equation based method is reverse-time migration, which provides the most accurate images of complex geological structures. Besides structural imaging, we can construct the angle-domain common-image gathers .

During the past decade extensive research has been carried out to understand the behaviour of the angle-domain common-image gathers (ADCIGs). It has been shown that ADCIGs not only provide the subsurface image, but could potentially be used to study the rock properties and fluid indicators by knowing the amplitudes of reflected waves as a function of incident angle at the interface. Common-image-gathers (CIGs) can also be generated in the offset-domain to perform amplitude-versus-offset (AVO) analysis but in complex geological settings such as - seismic imaging beneath gas, salt domes, and basalt structures - the ray field becomes multipathed therefore violating the assumptions of imaging in the offset-domain (Mahmoudian and Margrave (2009)). However ADCIGs uniquely define the rays as a function of angle for each point in the subsurface such that each event in the data is associated with only one subsurface location (Stolk and de Hoop (2001)).

In recent years, the research community proposed different methodologies to understand the imaging principles of generating the angle-domain common-image gathers (ADCIGs) (de Bruin et al. (1990); van Wijngaarden (1998); Rickett and Sava (2002); Sava and Fomel (2003); Kuhel and Sacchi (2003); Biondi and Symes (2004); Sava and Vasconcelos (2011)), where ADCIGs represents the seismic images as a function of the incidence angle. These authors computed the ADCIGs at various positions in the subsurface, commonly referred to as common-image points (CIP). The main steps proposed by these authors for generating the ADCIGs are: *i)* compute the *complete* source and receiver wavefields for *all* the sources; *ii)* construct the extended image at the predefined subsurface locations via a multidimensional correlation of the source and receiver wavefields along the subsurface offset axis; *iii)* compute ADCIGs by transforming the image gathers into the Radon domain. The computational cost of this approach is dominated by the number of sources and the number of subsurface offset samples. For this reason, one typically computes the image gathers at only a few subsurface points (CIP) for a limited range of subsurface offsets. So the question is: if we are not forming the full-image volume, can we avoid computing the *complete* wavefields for *all* the sources?

van Leeuwen and Herrmann (2012) addressed this question and showed that extended images can be computed efficiently for *all* subsurface offsets without explicitly calculating the source and receiver wavefields for *all* the sources. The main idea is to probe the full image volume for information by computing the action of the image volume on a vector that can be encoded with a certain subsurface position. These authors showed that instead of having to solve two PDEs for each source to obtain the source and receiver wavefields, we need to solve only two PDEs for each subsurface point at which we want to evaluate the extended image, thus making it computationally more feasible. We refer to full extended images as images as a function of all subsurface offsets and for all subsurface points using the full two-way wave-equation.

In this paper we use similar ideas to compute angle-domain image gathers that are aligned with the local dip from the action of these image volumes on vectors that encode the subsurface point of interest. We also propose a method to compute the local dip directly from the extended images. The goal is to conduct the amplitude-versus-angle (AVA) analysis on CIP gathers. The paper is organized as follows: First, we introduce the formulation of two-way wave-equation based forward modelling operator to generate time-harmonic seismic wavefield and its adjoint needed for extended imaging. Next, we show the formulation of angle-domain CIP gathers followed by the computation of local-dip information from CIP gathers. Finally, we test the quality of angle-domain CIP gathers on three different synthetic models.

EXTENDED IMAGING

Structural imaging is based on the principle that forward (source) and reverse propagated (receiver) wavefields coincide kinematically at time zero and coinciding subsurface source and receiver positions (zero offset). While this principle leads to high-resolution images, it does not provide information on the directional character of the reflected wavefield. Extended images, on the other hand, provide this information because they contain the response of the medium perturbations to sources and receivers that are no longer coincident with the location

of the medium perturbation. Following Berkhout (1984), we arrange the time-harmonic source and receiver wavefields into the matrices U and V, where each column corresponds to a source experiment. Given these matrices, the extended image at a *single frequency*, for *all* subsurface offsets and for *all* subsurface points can be written as the outer product of these two matrices, i.e., we have

$$E = VU^*, \tag{1}$$

where U,V are calculated using the two-way wave-equation. Figure 1 illustrates how different subsurface-offset gathers are embedded in the 4-dimensional image volume. In 2D, the extended image is a 5-dimensional function of *all* subsurface offsets and temporal shifts. So even in this case, it is prohibitively expensive to compute and store the extended image for all the subsurface points. To overcome this problem, we select l columns of E implicitly by multiplying this matrix with the tall matrix $W = [\mathbf{w}_1, \ldots, \mathbf{w}_l]$ yielding,

$$\widetilde{E} = EW, \tag{2}$$

where $\mathbf{w}_i = [0, \ldots, 0, 1, 0, \ldots, 0]$ represents a single scattering point with the location of 1 corresponding to i^{th} grid location of the point scatterer. Now each column of $\widetilde{E}$ represents a CIP gather at the locations represented by $\mathbf{w}_i$. We follow van Leeuwen and Herrmann (2012) to efficiently compute $\widetilde{E}$ by combining equations (1) and (2) as

$$\widetilde{E} = EW = H^{-*} P_r^T D Q^* P_s H^{-*} W, \tag{3}$$

where H is a discretization of the Helmholtz operator $(\omega^2 m + \nabla^2)$ with m is the squared slowness, The matrix Q represents the source function, $*$ represents the conjugate-transpose, D is the reflected data matrix and P_s, P_r samples the wavefield at the source and receiver positions (and hence, their transpose injects the sources and receivers into the grid). We can compute this product efficiently as follows

1. compute $\widetilde{U} = H^{-*} W$ and sample this wavefield at the source locations $\widetilde{D} = P_s \widetilde{U}$;
2. correlate the result with source function $\widetilde{Q} = Q^* \widetilde{D}$;
3. use the result as data weights $\widetilde{W} = D\widetilde{Q}$;
4. inject the wavefield $\widetilde{W}$ at the receiver locations and compute the extended image as $\widetilde{E} = H^{-*} P_r^T \widetilde{W}$.

The computational cost of calculating $\widetilde{E}$ is $2l$ PDE solves plus the cost of correlating the source and data matrices. Thus, the cost of computing the CIPs does not depend on the number of sources or the number of subsurface offsets, as it does in the conventional methods for computing image gathers (Sava and Vasconcelos, 2011). This is particularly beneficial when we are interested in computing only a few CIPs. An overview of the computational complexity is shown in Table 1.

Equation (3) defines an extended migration operator that maps the data matrix to an extended image. The corresponding extended demigration operator, $\mathscr{F}$, is defined as

$$\mathscr{F}(\tilde{E}) = P_r H^{-1} \widetilde{E} (Q^* P_s H^{-*} W)^*. \tag{4}$$

We can compute the action of $\mathscr{F}$ efficiently in a similar manner as described above for the extended migration operator. To compute reliable amplitudes for the extended image, we can estimate the least-squares extended image by solving

$$\underset{\tilde{E}}{\text{minimize}} \quad \frac{1}{2}\|D - \mathscr{F}(\tilde{E})\|_F^2. \tag{5}$$

In this paper, however, we use the adjoint of $\mathscr{F}$ (cf. equation (3)) in conjunction with filtering on the data and depth-scaling to compute the extended images. The scaling corrects for spherical spreading whereas the filtering makes the Hessian zero order by applying a half-integrations along the time axis (Herrmann et al., 2009).

	# of PDE solves	flops
conventional	$2N_s$	$N_s N_{h_x} N_{h_y} N_{h_z}$
this paper	$2N_x$	$N_r N_s$

Table 1: Computational complexity of the two schemes in terms of the number of sources N_s, receivers N_r, sample points N_x and desired number of subsurface offsets in each direction $N_{h_{\{x,y,z\}}}$.

ANGLE GATHERS IN THE RAY-PARAMETER DOMAIN

Since our goal is to conduct AVA analysis on a subset of subsurface points, we transform our CIP extended images into ray-parameter domain as proposed by de Bruin et al. (1990), with the ray parameter given by

$$p = \frac{k_x}{\omega} = \frac{\sin(\alpha)}{v}, \tag{6}$$

where k_x represents the horizontal wavenumber, v represents the local background velocity at the reflector and α represents the angle of incidence. Let $\mathbf{x}_i$ be a particular subsurface point at which we want to extract the angle gathers. As shown above we extract the corresponding CIP gather by selecting the corresponding column from the matrix E, which in turn can be done by multiplying the matrix with the i^{th} unit vector. Therefore, the CIP gather at $\mathbf{x}_i$ can be written as

$$e(\omega, \mathbf{x}_i, \mathbf{x}) = E(\omega)\mathbf{w}_i, \tag{7}$$

where $\mathbf{x}$ denotes any point in the subsurface, so that $\mathbf{x} - \mathbf{x}_i$ represents the subsurface offset in all directions. To get a meaningful angle gather, we select a subsurface offset (h) that is aligned with the local dip and define the angle gather as

$$I(\mathbf{x}_i, p, \theta) = \sum_{\omega} \sum_{h} e(\omega, \mathbf{x}_i, \mathbf{x}(h, \theta)) e^{\imath \omega p h}, \tag{8}$$

where $\mathbf{x}(h,\theta) = (h\cos\theta, h\sin\theta)$ and θ is the local geological dip. One of the difficulties in calculating the angle-gather is the pre-knowledge of θ. BrandsbergDahl et al. (2003) proposed a focusing method to estimate the local geological dip information. We use a similar idea to overcome this impediment by extracting the dip information by finding the dip that maximizes the stack-power.

$$\tilde{\theta} = \underset{\theta}{\text{argmax}} \sum_{h} \left| \sum_{\omega} e(\omega, \mathbf{x}_i, \mathbf{x}(h, \theta + \pi/2)) \right|. \tag{9}$$

Note that we are stacking along the offset that is perpendicular to the dip θ. The estimation of the dip can be done at almost no extra cost since we have all the subsurface offsets available.

To illustrate this method we consider a synthetic one-layer dipping model depicted in Figure 2(a). We extract a CIP gather at a point $x = 1750$ m and $z = 460$ m. We can see in Figure 2(b) that the CIP gather appears as a little dipole source that is aligned with the local dip. Since we are interested in the local directivity pattern of this dipole near the point of interest we perform the stack over narrow range of subsurface offsets. We can see in Figure 2(c) that for this one-layer dipping model, we get the maximum stack-power for a dip-angle of 12°, which is the true dip value. To show the efficacy of stack-power method, we will use this dip-information in the example section to compare the angle-dependent reflectivity coefficients with theoretical results. Finally, by repeating the above procedure for each depth level, we can form the angle gathers as a function of depth.

ANGLE DEPENDENT REFLECTIVITY ANALYSIS

To test the proposed algorithm for computing angle gathers, we extract the angle dependent reflectivity coefficients by taking the modulus of the angle gathers and compare them with the theoretical reflection coefficients as predicted by the (linearized) Zoeppritz equations. We consider three acoustic subsurface models; the first model has one-layer with constant density (Figure 3(a)); the second model has four-layers with the same medium properties as described in de Bruin et al. (1990) (Figure 4(a)); and the third model has one-dipping reflector (Figure 2(a)). We use a finite difference time-domain code (Symes et al., 2011) to generate the synthetic data sets. A peak frequency of 15Hz is used for the input Ricker wavelet. The reflection coefficients for the first model are displayed in Figure 3(b). We can see that the results match very well with the theoretical results. The results on the four-layer model are displayed in Figure 4. We can see that the reflection coefficients for the first and second reflector are well matched up to 50° and 40° and for the third and fourth reflector are matched up to 20°. The reason for this effects is the finite aperture. Finally, the results for the one-layer dipping model are shown in Figure 5. To show the effect of the dip on the angle gathers, we compute the angle-dependent reflectivity coefficients with no dip ($\theta = 0°$) and with the dip obtained via the method described above ($\theta = 12°$), which is also the true dip. We can clearly see the benefit of incorporating the dip-information in angle-domain image gathers.

DISCUSSION

We have presented an efficient way of forming angle-domain image gathers using two-way wave-equation based extended imaging. We followed the approach proposed by van Leeuwen and Herrmann (2012) to compute the image gathers for a few subsurface points without explicitly computing the source and receiver wave fields for all the sources. The main benefit of this approach is that the computational complexity mainly depends on the number of image points and not on the number of sources or desired number of subsurface offset samples. The resulting CIP gathers contain all possible subsurface offsets (horizontal, vertical, diagonal), therefore to get a meaningful angle gather, we select a subsurface offset that is aligned with the local dip. We also propose a method to extract the local dip information from the CIP gathers.

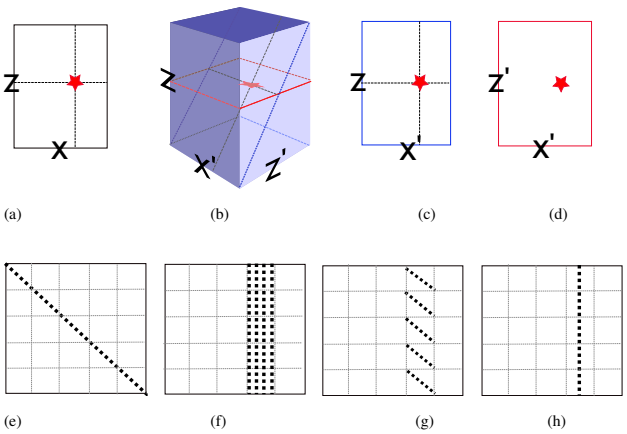

Figure 1: Different slices through the 4-dimensional image volume $e(z,z',x,x')$ around $z = z_0$ and $x = x_0$. (a) Conventional image $e(z,z,x,x)$, (b) Image gather for horizontal and vertical offset $e(z,z',x_0,x')$, (c) Image gather for horizontal offset $e(z,z,x_0,x')$ and (d) Image gather for a single scattering point $e(z_0,z',x_0,x')$. (e-g) shows how these slices are organized in the matrix representation of e.

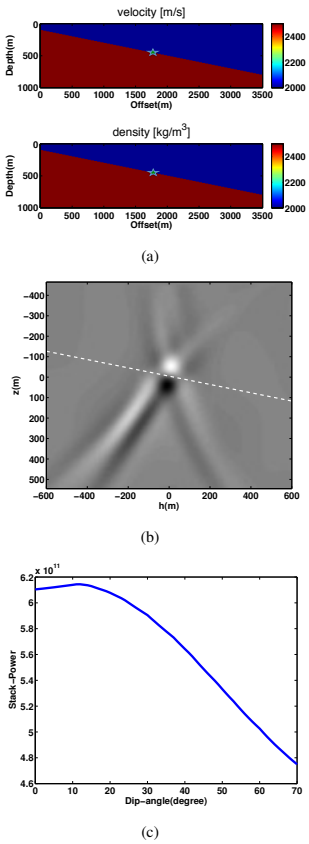

Figure 2: Estimation of local geological dip. (a) Dipping one-layer model overlay CIP location at $x = 1750$ m and $z = 460$ m indicated by star. (b) CIP gather overlay on dipping model. (c) Stack-power versus dip-angle. We can see the maximum stack-power corresponds to the dip value of 12°, which is the true dip value.

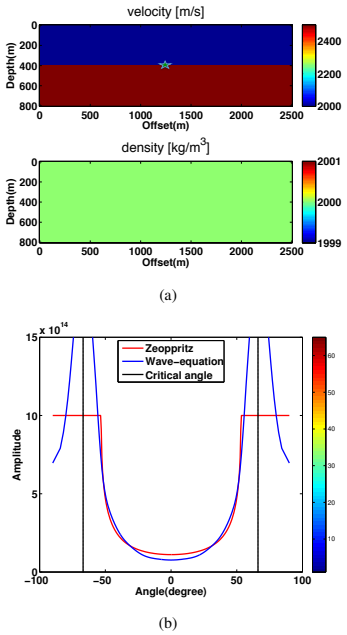

Figure 3: (a) Horizontal one-layer model overlay CIP location at $x = 1250$ m and $z = 400$ m indicated by star. (b) Modulus of angle-dependent reflectivity coefficients at CIP.

We illustrate the method on a few simple synthetic models and compare the angle-dependent reflection coefficients obtained from the angle gathers with the theoretical reflection coefficients as predicted by the (linearized) Zoeppritz equations. The examples show the potential benefits of incorporating the correct dip information. Future work is to cast the proposed methodology in a least-squares framework to compute reliable amplitudes for the extended images and test it on more complex geological models.

ACKNOWLEDGEMENTS

This work was in part financially supported by the Natural Sciences and Engineering Research Council of Canada Discovery Grant (22R81254) and the Collaborative Research and Development Grant DNOISE II (375142-08).This research was carried out as part of the SINBAD II project with support from the following organizations: BG Group, BGP, BP, Chevron, ConocoPhillips, Petrobras, ION GXT, CGGVeritas, Woodside, PGS, Total SA, and WesternGeco.

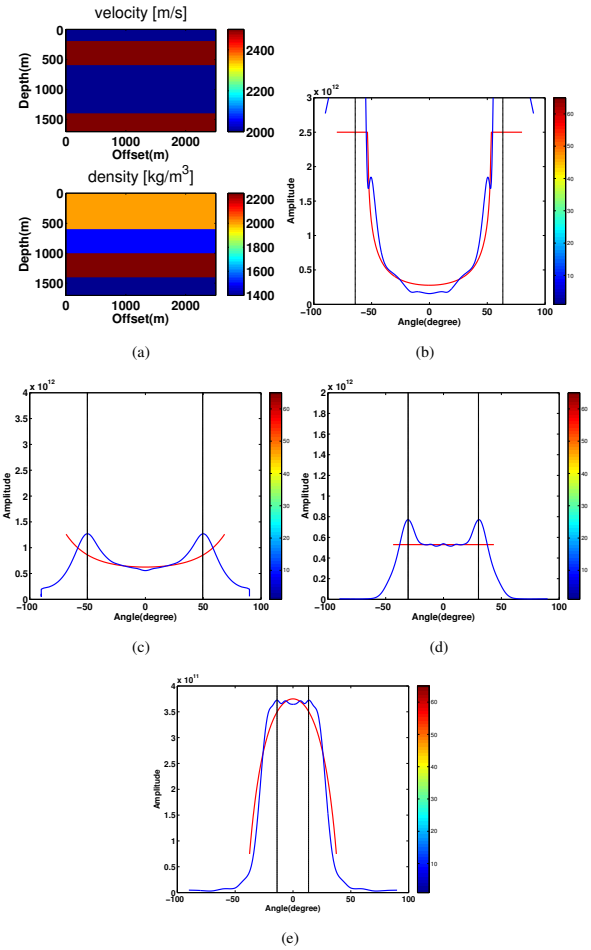

Figure 4: Angle dependent reflectivity coefficients in case of (a) horizontal four-layer model at $x = 1250$ m. Red curve represents the theoretical reflectivity coefficients, blue curve represents the wave-equation based reflectivity coefficients and black curve represents the critical-angle. (b) Modulus of angle-dependent reflectivity coefficients at $z = 200$ m. (c) Modulus of angle-dependent reflectivity coefficients at $z = 600$ m. (d) Modulus of angle-dependent reflectivity coefficients at $z = 1000$ m. (e) Modulus of angle-dependent reflectivity coefficients at $z = 1400$ m.

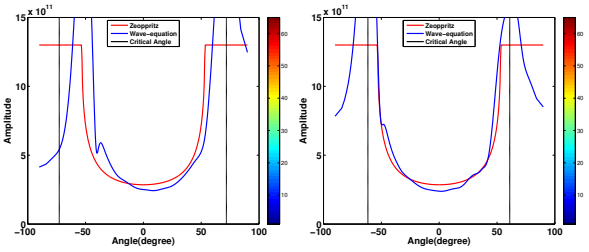

Figure 5: Modulus of angle-dependent reflectivity coefficients in dipping one-layer model at $z = 460$ m and $x = 1750$ m. Reflectivity coefficients (a) with no dip $\theta = 0^\circ$ and (b) with the dip obtained via the method described above ($\theta = 12^\circ$).

REFERENCES

Berkhout, A., 1984, Seismic migration: Imaging of seismic energy by wavefield extrapolation: Elsevier.

Biondi, B., and W. W. Symes, 2004, Angle-domain common-image gathers for migration velocity analysis by wavefield-continuation imaging: Geophysics, **69**, 1283.

Biondi, B. L., 2003, 3-D Seismic Imaging: Technical report, Stanford University.

BrandsbergDahl, S., M. de Hoop, and B. Ursin, 2003, Focusing in dip and ava compensation on scatteringangle/azimuth common image gathers: GEOPHYSICS, **68**, 232–254.

de Bruin, C., C. Wapenaar, and A. Berkhout, 1990, Angle dependent reflectivity by means of prestack migration: GEOPHYSICS, **55**, 1223–1234.

Herrmann, F. J., C. R. Brown, Y. A. Erlangga, and P. P. Moghaddam, 2009, Curvelet-based migration preconditioning and scaling: Geophysics, **74**, A41.

Kuhel, H., and M. Sacchi, 2003, Least-squares wave-equation migration for avp/ava inversion: GEOPHYSICS, **68**, 262–273.

Mahmoudian, F., and G. F. Margrave, 2009, A review of angle domain common image gathers: Technical Report.

Rickett, J., and P. Sava, 2002, Offset and angle domain common imagepoint gathers for shot profile migration: GEOPHYSICS, **67**, 883–889.

Sava, P., and S. Fomel, 2003, Angledomain commonimage gathers by wavefield continuation methods: GEOPHYSICS, **68**, 1065–1074.

Sava, P., and I. Vasconcelos, 2011, Extended imaging conditions for wave-equation migration: Geophysical Prospecting, **59**, 35–55.

Stolk, C., and M. de Hoop, 2001, Seismic inverse scattering in the 'wave-equation' approach: MSRI preprint 2001-047.

Symes, W. W., D. Sun, and M. Enriquez, 2011, From modelling to inversion: designing a well-adapted simulator: Geophysical Prospecting, **59**, 814–833.

van Leeuwen, T., and F. J. Herrmann, 2012, Wave-equation extended images: computation and velocity continuation: Presented at the EAGE technical program, EAGE, EAGE.

van Wijngaarden, A., 1998, Imaging and characterization of angle-dependent seismic reflection data.